The role of salinity on the dynamics of the Arabian Sea mini warm pool

Ebenezer S. Nyadjro,[1] Bulusu Subrahmanyam,[1,2] V. S. N. Murty,[3] and Jay F. Shriver[4]

Received 12 February 2012; revised 20 July 2012; accepted 20 July 2012; published 1 September 2012.

[1] Warmer (>28°C) sea surface temperature (SST) occurs in the South Eastern Arabian Sea (SEAS, 5°N–13°N, 65°E–76°E) during March–April, and is known as the Arabian Sea Mini Warm Pool (ASMWP). In this study, we address the role of salinity and the upper layer heat and salt budgets in the formation and collapse of this ASMWP. An assessment of Level 3 sea surface salinity (SSS) data from the Soil Moisture and Ocean Salinity (SMOS) satellite mission for the year 2010 shows that SMOS is able to capture the SSS variability in the SEAS. Analysis of temperature, salinity and currents from the Hybrid Coordinate Ocean Model during 2003–06, and, in situ temperature and salinity data from Argo floats during 2003–06 for the SEAS revealed that low salinity waters cap the top 60 m of the SEAS in January–February. This minimum salinity was concurrent with the formation of a barrier layer and with the time when the SEAS gained little net heat flux and the equatorward flowing East India Coastal Current (EICC) fed low saline waters into the SEAS. Subsequently, the net heat flux increased to a peak value under the increased salinity stratification, leading to the formation of the ASMWP in March–April. The ASMWP collapsed by May due to increase in SSS and the associated weakening of the salinity stratification. The monsoon onset vortex in May 2004 could be related to the minimum SSS that occurred in February 2004, followed by higher SST and heat content of the ASMWP in April 2004.

Citation: Nyadjro, E. S., B. Subrahmanyam, V. S. N. Murty, and J. F. Shriver (2012), The role of salinity on the dynamics of the Arabian Sea mini warm pool, *J. Geophys. Res.*, *117*, C09002, doi:10.1029/2012JC007978.

1. Introduction

[2] The oceanic regions with the sea surface temperature (SST) exceeding 28°C (Figure 1) are known as warm pools and are associated with deep atmospheric convection, low wind speed, heavy precipitation and low sea surface salinity (SSS) [*Gadgil et al.*, 1984; *Delcroix and McPhaden*, 2002; *Huang and Mehta*, 2004]. Small changes in SST lead to a significant response in the overlying atmosphere, resulting in global and regional climate changes through atmospheric teleconnections. The larger Indian Ocean Warm Pool (IOWP), extending from 20°S to 20°N (Figure 1), evolves independent of the smaller Arabian Sea Mini Warm Pool (ASMWP). The ASMWP, located in the South Eastern Arabian Sea (SEAS), attains its highest SST (~30°C) in March–April before the onset of the southwest monsoon leading to the belief that it plays an important role in the monsoon onset vortex formation [*Vinayachandran et al.*, 2007] and monsoon dynamics [*Vinayachandran and Shetye*, 1991; *Waliser*, 1996]. The ASMWP occurs with its core laying in the Lakshadweep Sea, the part of the SEAS between the Indian peninsula and the Lakshadweep islands to the west of the Indian mainland (Figure 1) [*Rao and Sivakumar*, 1999; *Shenoi et al.*, 1999]. Prior to the formation of the ASMWP, low saline waters are transported from the Bay of Bengal thereby causing higher stratification that reduces surface water cooling as a result of entrainment and leads to higher SSTs than are observed in the surrounding areas [*Shenoi et al.*, 2005; *Murty et al.*, 2006]. While the role of temperature in the formation and dynamics of the ASMWP has been extensively studied [*Rao and Sivakumar*, 1999; *Hareeshkumar et al.*, 2005; *Shenoi et al.*, 2005], the effects of salinity are understudied.

[3] Studies on the seasonal and interannual variability of salinity in the ASMWP region are limited. Salinity effects complicate the air-sea interactions over the warm pool region, and there appears to be an important feedback between SST, precipitation, upper ocean salinity, and wind-induced mixing [*Vinayachandran et al.*, 2007; *Nisha et al.*, 2009]. In the warm pool region of the SEAS, the surface layer is characterized with lower salinity waters. This warm and low salinity region is in turn characterized with a shallow Mixed Layer

[1]Marine Science Program, University of South Carolina, Columbia, South Carolina, USA.
[2]Department of Earth and Ocean Sciences, University of South Carolina, Columbia, South Carolina, USA.
[3]National Institute of Oceanography Regional Center, Council of Scientific and Industrial Research, Visakhapatnam, India.
[4]Naval Research Laboratory, Stennis Space Center, Mississippi, USA.

Corresponding author: E. S. Nyadjro, Marine Science Program, University of South Carolina, 701 Sumter St., EWS 617, Columbia, SC 29208, USA. (enyadjro@geol.sc.edu)

0148-0227/12/2012JC007978

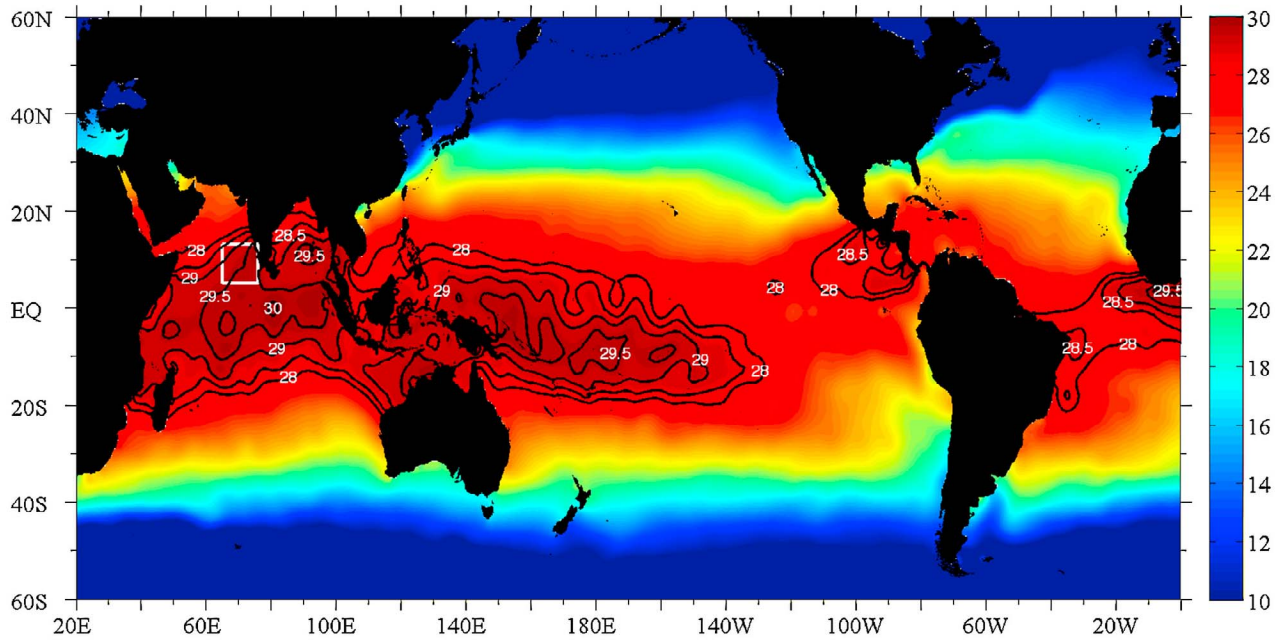

Figure 1. Mean SST (°C) for March–April from Argo data set showing the larger warm pool and ASMWP in the SEAS region (5°N–13°N, 65°E–76°E, shown by white box). SST greater than 28°C is contoured. Contour interval is 0.5°C.

Depth (MLD), which comes into contact with the overlying atmosphere and modifies the air-sea interaction processes [*Krishna Kumar et al.*, 2005; *Murty et al.*, 2006]. Over this warm, low salinity, shallow mixed layer, intense convection takes place; thus this region contributes to both oceanic and atmospheric processes. Due to the paucity of salinity time series measurements, our understanding of the critical influence of salinity at different time scales on the upper ocean processes and their impact on the atmospheric convection at a synoptic scale (e.g., monsoon depressions, tropical cyclones), and monsoon activity have been limited. The launch of the Soil Moisture and Ocean Salinity (SMOS) mission by the European Space Agency (ESA) in November 2009 and Aquarius/SAC-D salinity mission by the U.S. NASA and Space Agency of Argentina (Comision Nacional de Actividades Espaciales, CONAE) in June 2011 are expected to provide satellite-derived global measurements of SSS. One motivation for this study is to assess the ability of SMOS to capture the import of low saline waters into the SEAS region, a precursor for the ASMWP salinity-influenced dynamics. Unlike SST, ocean salinity does not directly affect the atmosphere. However, in some regions salinity plays an important role in setting up upper ocean stratification, which, along with surface fluxes, controls SST variability. Ocean dynamics, which may contribute to the upper ocean heat budget, are also affected by salinity. In this paper, we examine the critical role of salinity in the formation and dynamics of the ASMWP.

[4] The rest of the paper is organized as follows: in section 2, we introduce the data sets used, and formulae and methods for computation of the salt and heat budgets. In section 3, we present results and discussion of near-surface patterns of SSS from SMOS, Argo and Hybrid Coordinate Ocean Model (HYCOM), sub-surface variability of salinity and temperature from Argo and HYCOM, and variability of salt and heat budget terms. Finally, in section 4, we provide a summary of the results of this study.

2. Data and Methods

2.1. Data

[5] In this study, we used the available Level 3 SMOS SSS data for the year 2010 obtained from the Ocean Salinity Expertise Center (CECOS) of the CNES-IFREMER Centre Aval de Traitemenent des Donnees SMOS (CATDS), at IFREMER, Plouzane (France). This data is available on a 0.5° × 0.5° grid. The onboard SMOS passive microwave radiometer estimates salinity from the brightness temperature (T_B) of the sea surface using the L-band (1400–1427 MHz) frequency [*Font et al.*, 2004, 2010; *Camps et al.*, 2005]. The Level 3 maps are computed using a simplified image reconstruction algorithm, spatial and temporal aggregation of T_B and correction for instrument errors (calibration), foam cover, geophysical parameters (e.g., surface roughness, sun and moon glint) and radio frequency interference-RFI [*Font et al.*, 2004; *Oliva et al.*, 2012]. At present, it is not possible to properly retrieve salinity within about 100 km from the coast.

[6] We used the gridded Argo salinity and temperature data obtained from Coriolis (http://www.coriolis.eu.org). This global data is produced in real time by optimal interpolation with spatial resolution of 0.5° × 0.5°. The Argo floats are one of the main sources of in situ salinity observations. As of May 2012, there were about 770 of these floats in the Indian Ocean. The floats travel to about 2000 m depth and come up to the surface every 10 days to transmit data [*Riser et al.*, 2008]. The floats are capable of measuring salinity up to a

global accuracy of 0.01 psu [*Wong et al.*, 2003]. A study by *Kobayashi and Minato* [2005] of the eastern tropical Indian Ocean shows that Argo accuracy was within ±0.01 psu even up to 1000 db. *Huang et al.* [2008] reported that the least accuracy from Argo is observed in the eastern tropical Indian Ocean, thus the accuracy for the entire Indian Ocean can be considered to be within the expected global accuracy of 0.01 psu.

[7] In this study, we made use of the outputs from the high resolution HYCOM for the 2003–2006 period. HYCOM is a 1/12° horizontal resolution (~7 km at midlatitudes and 3.5 km at the North Pole) and 32 hybrid layers in the vertical, is isopycnal in the open stratified ocean, and makes a smooth transition to a terrain-following (σ) coordinate in coastal waters using the layered continuity equation [*Bleck*, 2002]. The model's use of varying vertical coordinates allows it to effectively simulate the characteristics of ocean circulation as well as interior water mass distribution. These features are very important especially in the study of transport of ocean properties such as salinity, as the dynamics are strongly influenced by localized processes hence the use of a fixed depth will be inefficient [*Chassignet et al.*, 1996]. HYCOM has the capability of selecting among several different vertical mixing sub-models; this version uses K-Profile Parameterization (KPP) [*Large et al.*, 1994]. This feature is essential for our study, as salinity distribution, especially in the surface ocean, is partly dependent on vertical mixing.

[8] This version of HYCOM was initialized using monthly mean temperature and salinity from the 1/4° Generalized Digital Environmental Model (GDEM4) climatology [*Carnes et al.*, 2010] in January. This experiment was then run for 13 years using climatological monthly mean wind and thermal forcing constructed from the 0.3125° NCEP Climate Forecast System Reanalysis (CFSR) over the 1993–2009 time frame. In addition, 6-h variability from CFSR over the period January 2002–December 2003 was added to the climatological wind-forcing (but not the thermal forcing) to add the higher frequency variability needed for realistic simulation of the surface mixed layer. In order to keep the evaporation minus precipitation budget on track, the model weakly relaxes to monthly mean SSS from the Polar Science Center Hydrographic Climatology (PHC) SSS. The actual SSS relaxation e-folding time depends on the MLD and is (30 days × 30 m/MLD m) days, i.e., it is more rapid when the MLD is shallow and less so when it is deep. This virtual salt flux is sufficient to avoid long-term drift in SSS, but not so strong as to inhibit SSS anomaly formation. The SSS relaxation is in addition to the evaporation-precipitation budget.

[9] Once the model was determined to be equilibrated after being spun-up with climatological forcing, the simulation was then continued using 1 hourly NCEP CFSR, heat fluxes and precipitation fields for the period 1993–2010 as the forcing. Monthly varying discharge from 986 global rivers is included as a surface precipitation flux (but not as a volume flux). There is no assimilation of any ocean data, including SST, and no relaxation to any other data except SSS to keep the evaporation minus precipitation balance on track. Because we are using the global version of HYCOM, there is no sponge layer across the lateral boundaries. The model allows the Indonesian Throughflow (ITF) to flow into the Indian Ocean, enabling salt to be conserved in the steady state while potentially varying from year to year.

[10] We analyzed the solar radiation and heat fluxes using Objectively Analyzed air-sea Heat Fluxes (OAFlux) Version 3 data [*Yu et al.*, 2007] available on a 1° × 1° grid for the period 2003–2006. The OAFlux products are constructed from an optimal blending of satellite retrievals and three atmospheric reanalyzes. Daily fluxes are computed from the optimally estimated variables using the COARE bulk flux algorithm 3.0. OAFlux evaporation data was used in salt budget estimation.

[11] Precipitation data for this study was obtained from the Global Precipitation Climatology Project (GPCP) data set [*Adler et al.*, 2003]. The GPCP data set is produced from measurements from rain gauges and satellite infrared and microwave sensors and is available on a 2.5° × 2.5° grid.

[12] We define and compute the MLD as the depth where the water density is higher by 0.2 kg.m^{-3} than the surface density [*McPhaden et al.*, 2009]. Similarly, the isothermal layer depth (ILD) is defined as the depth at which the temperature changes by 1°C from the temperature at the ocean surface.

[13] For consistency, the data sets in this study were re-gridded onto a common grid (2.5° × 2.5°) using linear interpolation.

2.2. Methods

[14] Following *Delcroix and Henin* [1991], *Rao and Sivakumar* [2003] and *Foltz and McPhaden* [2008], the mixed layer salt budget can be written as

$$\frac{\partial S}{\partial t} = h^{-1}(E-P)S - \left(U\frac{\partial S}{\partial x}\right) - \left(V\frac{\partial S}{\partial y}\right) - W_e.(S - S_{z=h})h^{-1} + R, \quad (1)$$

where S is mixed layer salinity, h is the depth of the upper mixed layer, E is evaporation, P is precipitation, U is zonal component of velocity, V is meridional component of velocity, W_e is entrainment velocity, and $S_{z=h}$ is the salinity just below the MLD. The terms in equation (1) from left to right are the salinity tendency, sea surface freshwater flux, zonal salt advection, meridional salt advection, entrainment and residuals (R) which represents physical processes that are unaccounted for. We split the horizontal (zonal and meridional) advection into Ekman drift and geostrophic current components in order to understand their relative roles, magnitudes and effects in the salt balance of the SEAS region (white box in Figure 1). Geostrophic component of the horizontal salt advection was estimated from

$$U_{gs} = U_g\frac{\partial S}{\partial x} \text{ and } V_{gs} = V_g\frac{\partial S}{\partial y}, \quad (2)$$

where U_g and V_g are the surface geostrophic current components computed respectively from

$$U_g = -\frac{g}{f}\frac{\partial \zeta}{\partial y} \text{ and } V_g = \frac{g}{f}\frac{\partial \zeta}{\partial x}, \quad (3)$$

where ζ is sea surface height (SSH) from TOPEX/Poseidon and Jason altimetry data, g is acceleration due to gravity (9.8 ms^{-2}) and f is the Coriolis parameter ($2\Omega\sin\phi$, where Ω is the angular velocity of the Earth).

[15] The Ekman wind drift components of the horizontal salt advection was estimated from

$$U_{es} = U_e \frac{\partial S}{\partial x} \text{ and } V_{es} = V_e \frac{\partial S}{\partial y}, \quad (4)$$

where U_e and V_e are the surface Ekman drift components computed respectively from

$$U_e = \frac{\tau_y}{\rho_o fh} \text{ and } V_e = \frac{-\tau_x}{\rho_o fh}, \quad (5)$$

where the surface wind stress $\tau = \rho_a C_D \psi$ was computed using the $1^\circ \times 1^\circ$ gridded pseudostress (ψ) data set with air density ρ_a = 1.2041 kg m^{-3} and drag coefficient C_D = 0.0015 [*Bourassa et al.*, 2005] from the Florida State University's (FSU) Center for Ocean-Atmosphere Prediction Studies (COAPS). ρ_o is the water density (1023 kg m^{-3}).

[16] We computed the entrainment velocity, W_e, following *Stevenson and Niiler* [1983],

$$W_e = H\left(\frac{\partial h}{\partial t} + \nabla.h\boldsymbol{\nu}\right), \quad (6)$$

where $\boldsymbol{\nu}$ is the horizontal velocity and H is the Heaviside unit function [=0 if (W_e + dh/dt < 0, =1 if (W_e + dh/dt > 0]. By this, only the entrainment (positive) velocity is considered whiles the detrainment (negative) velocity is not considered. This is because the water that flows out from the bottom of the mixed layer has approximately the same characteristics as the water in the mixed layer and hence will not affect the salinity in the mixed layer [*Ren and Riser*, 2009].

[17] Following *Swenson and Hansen* [1999] and *Kurian and Vinayachandran* [2007], the mixed layer heat budget can be written as

$$\frac{\partial T}{\partial t} = \frac{Q_s}{\rho_o C_p h} - \left(U\frac{\partial T}{\partial x}\right) - \left(V\frac{\partial T}{\partial y}\right) - (W_e \Delta T)h^{-1} + D, \quad (7)$$

where T is the vertically averaged HYCOM temperature over the depth of upper mixed layer, h, Q_s is the near-surface heat flux, C_p is the specific heat capacity of seawater (4.0×10^3 J kg^{-1} K^{-1}), U is HYCOM zonal component of velocity, V is HYCOM meridional component of velocity, ΔT is the difference between the vertically averaged temperature of the mixed layer and the temperature just below the mixed layer, W_e is the entrainment velocity and D represents the residual term which includes processes which we could not estimate directly from the data such as diapycnal mixing and diffusion. In the first term of equation (7), we have not considered the penetrative solar radiation as suggested by *Sengupta et al.* [2008].

[18] The heat content (H) of the upper 40 m layer in the SEAS was computed from HYCOM simulations using the following relation:

$$H = \int \rho_o C_p T dz, \quad (8)$$

where T is mean temperature over depth interval of dz.

[19] In our estimations of the salt and heat budget (equations (1) and (7)), monthly averaged parameters were used. First, all terms were expanded as a time average plus a departure from the time average. For example, salinity was expanded as $S = \bar{S} + S'$(i.e., monthly average + departure from average). All the terms involving departures from the time average are then combined into the "residual" term, which represents the difference between the tendency terms (left hand side) and budget terms (right hand side) of equations (1) and (7).

3. Results and Discussion

3.1. Comparison Between SMOS, Argo and HYCOM Sea Surface Salinity

[20] We evaluate HYCOM SSS using Argo SSS. We additionally assess the ability of the SMOS satellite to capture the exchange of SSS between the Arabian Sea and the Bay of Bengal via the SEAS region. Recently, *Subrahmanyam et al.* [2012] discussed the general characteristics of Indian Ocean SMOS-derived SSS on seasonal time scales. We present here the selected monthly SSS distributions in 2010 derived from SMOS, Argo and HYCOM in the northern Indian Ocean (Figures 2a–2h). The general characteristics of SSS are well captured in all three SSS products. In the northern Indian Ocean, the Bay of Bengal has lower SSS as a result of precipitation exceeding evaporation and the influx of river-runoff, whereas the Arabian Sea has higher SSS as a result of evaporation exceeding precipitation [*Prasad and Ikeda*, 2002; *Joseph and Freeland*, 2005; *Nyadjro et al.*, 2011]. Additionally, the Arabian Sea is semi-enclosed, bounded on three sides by landmasses with connections to the highly saline Persian Gulf and Red Sea. Salinity in the northern Indian Ocean is partly balanced by salt exchange between the Arabian Sea and Bay of Bengal via the monsoon-influenced seasonal reversing currents [*Schott and McCreary*, 2001; *Rao and Sivakumar*, 2003; *Nyadjro et al.*, 2010]. The waters exchanged between these two basins pass through the SEAS region and affect the salt budget in the ASMWP.

[21] Although SMOS is not able to resolve the SSS along the coastal regions (Figures 2a, 2d, 2g, and 2j), nevertheless, the arrival of low saline waters from the Bay of Bengal into the SEAS region is well captured (Figure 2g). The SMOS-observed SSS shows the occurrence of the lowest SSS in December–February in the SEAS region (Figures 2d and 2g). Bay of Bengal also contributes to the freshwater advection to the southern tropical Indian Ocean along the coast of Sumatra (Figure not shown).

[22] The HYCOM simulated current vectors are superimposed on the HYCOM SSS map (Figures 2c, 2f, 2i, and 2l). During the winter (Figures 2a–2f), less saline waters from the Bay of Bengal are advected by the southward flowing East India Coastal Current (EICC) into the West India Coastal Current (WICC) via the westward flowing Northeast Monsoon Current (NMC) [*Vinayachandran et al.*, 1999; *Subrahmanyam et al.*, 2011]. These broader currents are depicted schematically in Figures 2b, 2e, 2h, and 2k. The low saline waters imported into the SEAS region become noticeable in December (Figures 2d–2f) and peaks by February (Figures 2g–2i). It is worth mentioning that this is better captured by SMOS (Figure 2g) than Argo (Figure 2h) and

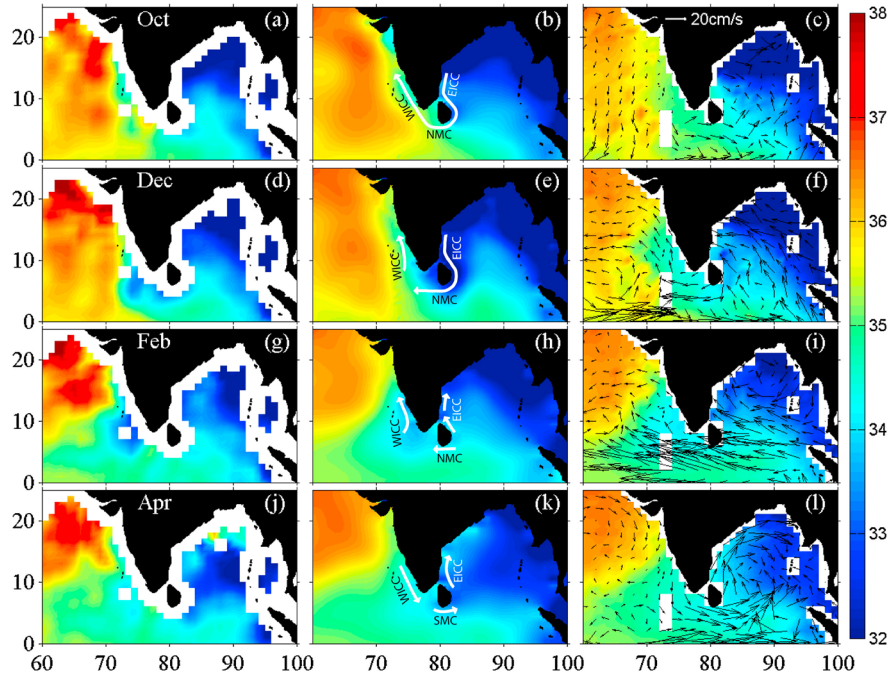

Figure 2. Selected monthly maps of sea surface salinity (SSS) for (a, d, g, and j) SMOS, (b, e, h, and k) Argo and (c, f, i, and l) HYCOM (superimposed with HYCOM near-surface currents) for October, December, February, and April 2010. The white arrows (in Figures 2b, 2e, 2h, and 2k) show a schematic of the pathways of the major currents in the region: EICC, the East India Coastal Current, WICC, the West India Coastal Current, NMC, the Northeast Monsoon Current and SMC, the Southwest Monsoon Current.

HYCOM (Figure 2i). The differences between SMOS SSS and Argo SSS and HYCOM SSS are to be expected as SMOS measures salinity at the surface skin layer of the ocean as compared to SSS estimated at about 5 m below surface as is the case with HYCOM and Argo. By April (Figures 2j–2l), the highly saline Arabian Sea Water mass spreads with the eastward flowing Southwest Monsoon Current (SMC) and advects salty water into the Bay of Bengal [*Morrison*, 1997; *Schott and McCreary*, 2001].

3.2. Near-Surface SSS and SST Variability in the SEAS From HYCOM and Argo

[23] Seasonal variations of SEAS box-averaged SSS and SST for 2003–2006 from HYCOM output show reasonable

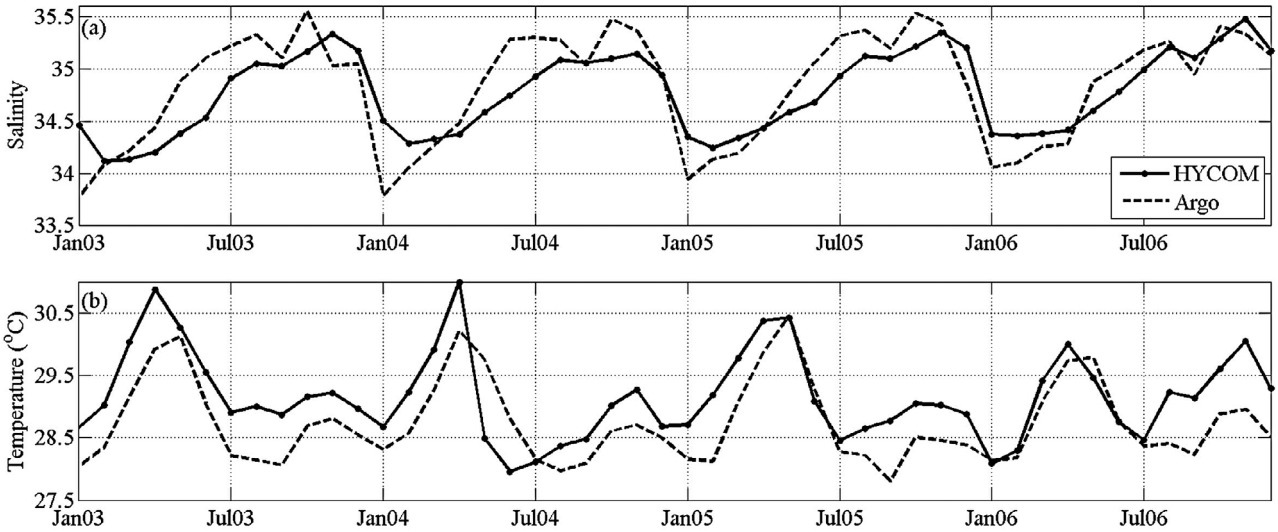

Figure 3. Seasonal variations of (a) SSS and (b) SST for the SEAS region from HYCOM (bold line) and Argo (dashed line).

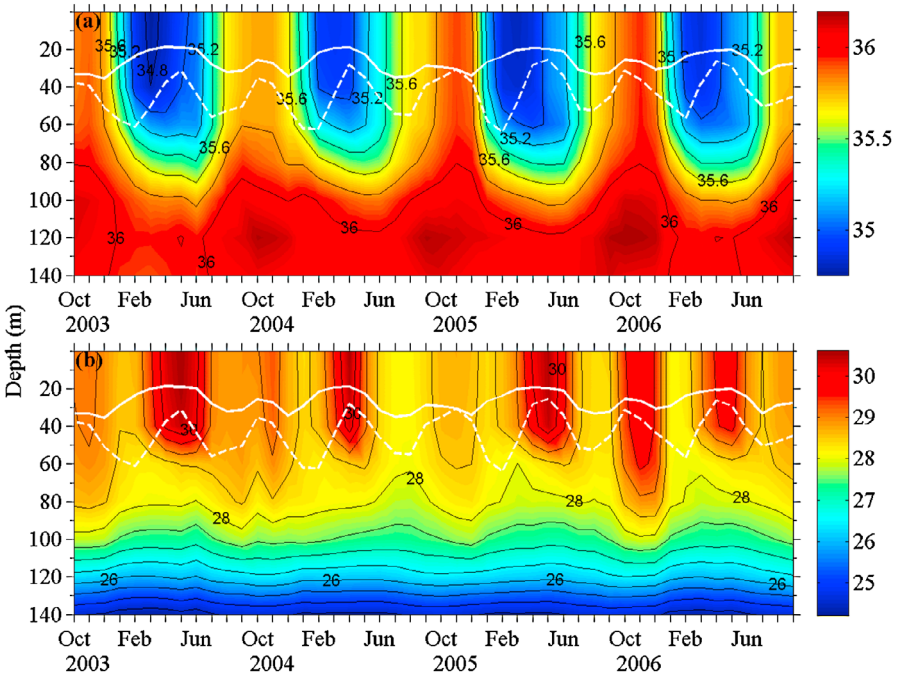

Figure 4. Depth-time sections of SEAS box-averaged (a) HYCOM salinity and (b) HYCOM temperature during October 2003–September 2006 for the SEAS region (see white box in Figure 1). The mixed layer depth (solid white line) and isothermal layer depth (dashed white line) are overlaid. Contour interval is 0.2 psu and 0.5°C, respectively, for salinity and temperature.

agreement with Argo in situ data, although HYCOM SSS tends to be a little lower than Argo SSS (Figure 3a) and HYCOM SST tends to be a little higher than Argo SST (Figure 3b). These combinations of SSS and SST in both data sets represent the same lesser density surface waters. The seasonal cycles of SSS show that the low salinity waters from the Bay of Bengal are advected into the SEAS region by January–February, 2 months prior to the SST warming in April. This 2 months lag implies that the advection of low salinity waters is a precursor for the SST warming with the strong salinity stratification [*Shenoi et al.*, 1999]. During the SW monsoon season, the SMC brings high saline waters from the northern Arabian Sea to the south and SEAS region through the equatorward flowing WICC. These high salinity waters (>35psu) continues to flow into the SEAS till the beginning of the northeast monsoon (winter monsoon). The seasonal cycles of SSS and SST further show that the minimum and maximum SSS values appear to increase from one year to the other, while the minimum and maximum SST tend to decrease during 2003–2006 period in the SEAS region. This trend suggests that the stratification in the upper layer water column is weakened in the recent years in the SEAS region, which in turn would have an impact on the air-sea interaction processes (highlighted in the discussion below). This further highlights the extensive contribution of presence of low salinity waters in the SEAS on the variation of SST maximum. The occurrence of anomalously low SSS and anomalously high SST in 2004 can be attributed to the occurrence of a monsoon vortex in that year. This is further discussed in section 3.5.

3.3. Sub-Surface Ocean Salinity and Temperature Variability in the SEAS

[24] The depth-time sections of salinity and temperature constructed using HYCOM simulations (Figures 4a and 4b) and Argo data (Figures 5a and 5b) are presented for the SEAS region for the 2003–2006 period. Comparison of the model and in situ data shows general agreement in the salinity and temperature structures. The average depth of the warm pool is about 50 m. Low saline waters occupy the top 60 m layer between December and June with a peak of this freshwater occurring during February (Figures 4a and 5a). In HYCOM simulations, higher salinities (>36 psu) occur below 90 m between July and December with a high salinity core observed during September–October. In Argo data, higher salinities (>36 psu) occur in the 20–100 m layer during July–December. Two warm cores are observed (Figures 4b and 5b); the primary warm core (>30°C) occurs between April and May while the secondary warm core (~29°C) is observed during October–December.

[25] Besides the significant seasonal variability that is observed in the vertical sections of salinity and temperature, there is interannual variability in the salinity and temperature structures in the upper 140 m (Figure 4 and 5). As an example, the HYCOM upper layer salinity is lowest in February 2003 and relatively higher in February 2006 (Figure 4). Correspondingly, one would see the warmest temperatures in the upper 50 m in April 2003 and relatively lesser warm waters in April 2006. By June, there is an upward movement of the thermocline causing entrainment of colder waters into the mixed layer whereas the freshwaters penetrate to deeper depths due to mixing. In these vertical sections, the time

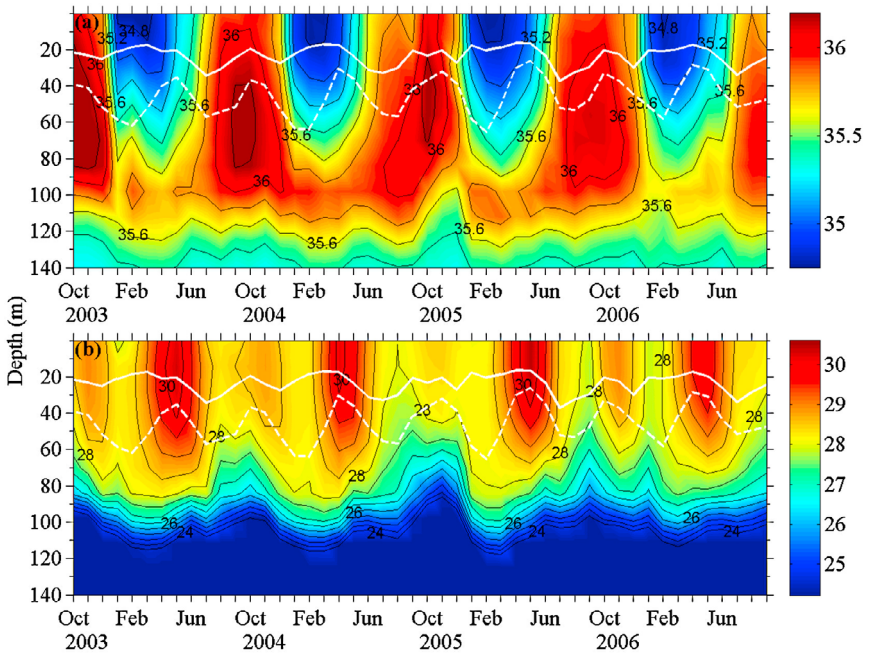

Figure 5. Depth-time sections of SEAS box-averaged (a) Argo salinity and (b) Argo temperature during October 2003–September 2006 for the SEAS region (see white box in Figure 1). The mixed layer depth (solid white line) and isothermal layer depth (dashed white line) are overlaid. Contour interval is 0.2 psu and 0.5°C, respectively, for salinity and temperature.

variation of MLD and ILD are also displayed. The pattern of variations in MLD and ILD are similar in both HYCOM simulations and Argo data (Figures 4 and 5). The MLD is shallow (~20–30 m depth) in the freshwater pool in winter months, whereas the ILD is deep (up to 60 m depth) resulting in the larger (40 m thick) barrier layer thickness (the layer showing the depth difference between the ILD and MLD). At the time of development of the warm pool by April–May, the barrier layer thickness becomes small (~20 m). Once again, by October, when the SSS reaches higher values, the barrier layer thickness reduced to around 10 m.

[26] Seasonal vertical profiles of temperature and salinity in February (winter), April (pre-SW monsoon) and October (post-monsoon) are shown for HYCOM simulations (Figures 6a–6c) and Argo data (Figures 6d–6f). There are differences between the HYCOM profiles and the Argo profiles. For example, the temperature at 140 m is about 24°C in HYCOM whereas it is about 19°C in Argo. Similarly whiles the HYCOM salinity in the entire layer varied between 34.2 and 35.7 in February, the variation was weak in Argo (between 34.7 and 35.8). Additionally, in the Argo profiles, subsurface salinity maximum occur at 100 m whereas this feature is absent in HYCOM salinity. The formation of a barrier layer occurs in winter (February) (Figure 6a) with the lowest surface salinity waters during the peak of advection of low saline waters by the EICC and the WICC. During April at the time of highest SST (>30.5°C) in the SEAS, low salinity waters extend to about 40 m intensifying the stratification that reduces cooling as a result of entrainment (Figure 6b). During the post-monsoon (October), barrier layer is not present as significant change in temperature and salinity with depth begins to occur at about 60 m (Figure 6c). The SSS attains a

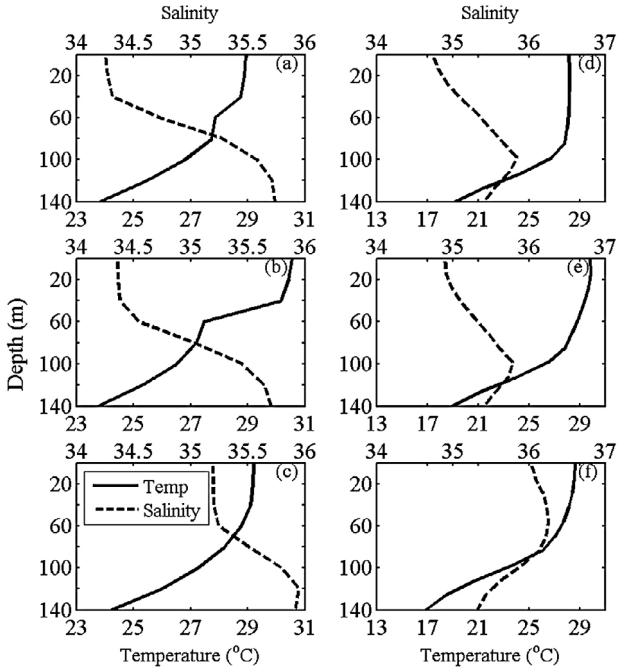

Figure 6. Vertical profiles of SEAS box-averaged salinity and temperature using (a–c) HYCOM simulations and (d–f) Argo data for the SEAS region (see white box in Figure 1) for February (winter, Figures 6a and 6d), April (pre-SW monsoon, Figures 6b and 6e) and October (post-monsoon, Figures 6c and 6f). Large temperature and salinity changes are noticed in the thermocline (below 80 m depth) in the Argo data set compared to that of HYCOM simulations.

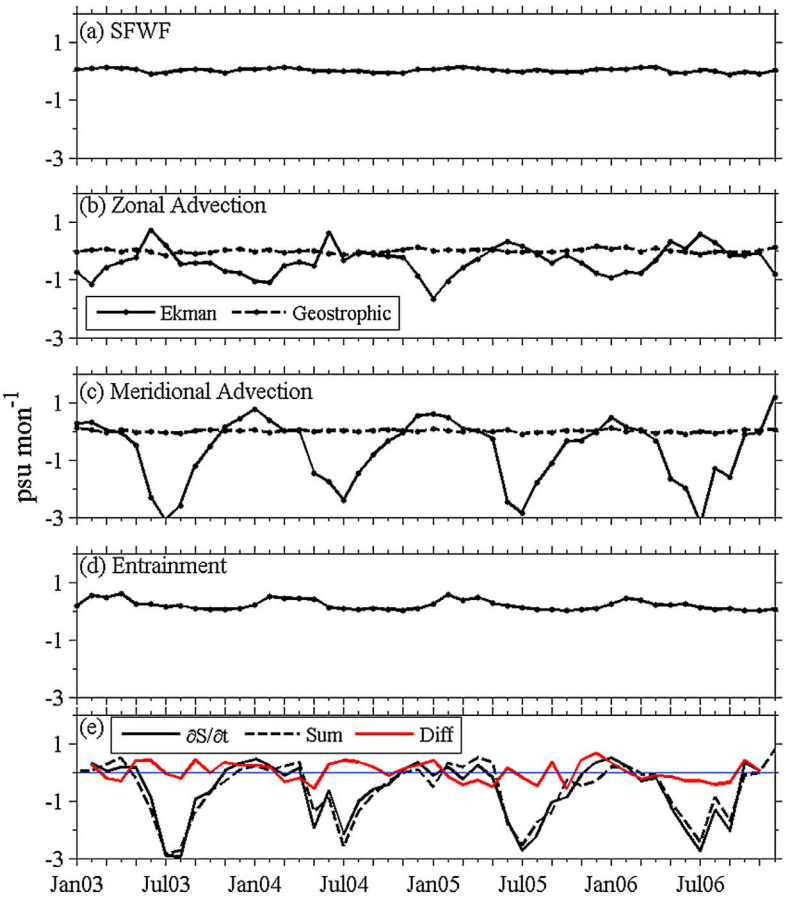

Figure 7. Seasonal variations of SEAS box-averaged salt budget terms in the SEAS region (refer to white box in Figure 1): (a) surface freshwater forcing term; (b) zonal advection; (c) meridional advection; (d) entrainment, based on the HYCOM simulations and FSU-COAPS generated pseudo-wind stress data and (e) the salinity tendency (solid black line representing the left hand side of equation (1)), the sum of salt budget terms (dashed black line representing the right hand side of equation (1)), the residual (difference between the salt tendency and the salt budget terms) of equation (1).

higher value of 35.2 psu in October compared to the lowest SSS in February (Figures 6c and 6a). This is consistent with the idea that barrier layer formation is essential for warm pool formation in the SEAS region. It is likely that low salinity water advected from the Bay of Bengal into the SEAS region reduces the mixed layer thickness here, and helps 'trap' heat due to solar radiation, amplifying surface heating.

3.4. Salt Budget of the SEAS

[27] We have further analyzed the salt budget of the SEAS region for the 2003–2006 (Figure 7) in order to examine the relative roles of Ekman salt advection and geostrophic salt advection in the dynamics of the ASMWP. The surface freshwater term, E-P (Figure 7a), also the local forcing, contributes the least to the salt budget while the horizontal advection terms (Figures 7b and 7c) contribute the most to the salt budget. Of the horizontal salt advection terms, the zonal Ekman component and meridional Ekman component have larger magnitudes and contribute to the advective forcing. In winter, the zonal Ekman component of the salt advection is large while in the summer the meridional Ekman component of the salt advection is large (Figures 7b and 7c). This emphasizes the important role of local surface wind-forcing in the salt advection and salt budget of the SEAS region. The weaker northward meridional Ekman salt advection and larger westward zonal Ekman salt advection during winter period contribute to the advection of low salinity waters into the SEAS. At the peak of the SW monsoon, the zonal Ekman salt advection is weak and westward (Figure 7b) and meridional Ekman salt advection is large and directed southward (Figure 7c), contributing to the salt removal from the SEAS region. The contribution of entrainment (Figure 7d) to the salt budget is higher during the winter months and minimum during the SW monsoon.

[28] The sum of the salt budget terms (right hand side of equation (1)), underestimates the mixed layer salinity tendency in most months of the study period by magnitudes of $\pm$0.5 psu (Figure 7e). These residuals arise from unresolved physical processes such as turbulent mixing and eddy processes. Turbulent mixing, which includes turbulent entrainment and diffusion, could be important for salt balance in the mixed layer especially during the presence of thick barrier layers as the subsurface is a source of high salinity [*Foltz and McPhaden*, 2008]. In our study for example, we observed

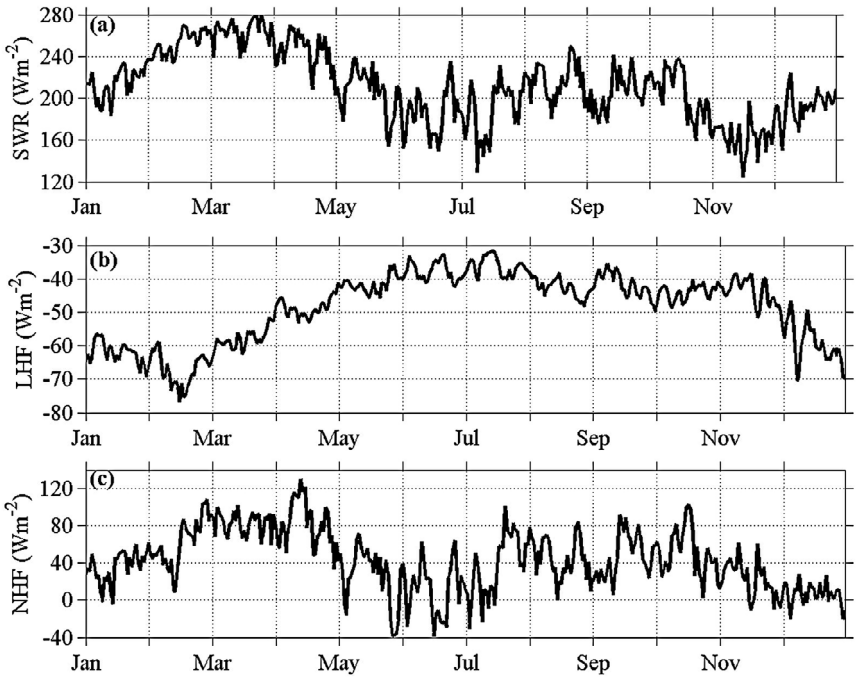

Figure 8. Annual variations of (a) short wave radiation (SWR), (b) Latent heat flux (LHF) and (c) net heat flux (NHF) at the sea surface averaged for the SEAS region, based on the daily averages of OAFlux climatology. Positive (negative) NHF denotes heat gain (loss) at (from) the sea surface.

thicker barrier layers in the freshwater pool during winters. The residuals can also be attributed to errors in the data sets that we used to compute the salt budget terms especially in the estimation of horizontal advection, the largest contributor to the salt budget in the SEAS. For the horizontal advection estimations, we have computed the Ekman and geostrophic current components using the COAPS winds products and altimetry data, respectively, rather than the HYCOM simulated current velocities.

3.5. Heat Budget of the SEAS

[29] To understand the role of the solar radiation, air-sea heat fluxes and net heat flux at sea surface on the formation of ASMWP in the SEAS, we analyzed the solar radiation and heat flux data (Figure 8) of the daily averaged OAFlux climatology [*Yu et al.*, 2007]. The short wave radiation at the sea surface is large ($\sim$280 W.m^{-2}) in March–April (Figure 8a) and decreases to a lower value ($\sim$160 W.m^{-2}) during SW monsoon (June–July) in association with the monsoon clouds. The latent heat flux is large (-60 to -75 W.m^{-2}) during winter (January–February) and gradually decreases to -30 W.m^{-2} during SW monsoon (Figure 8b). The net heat flux (NHF) (=Qs-Qb-Qe-Qh, where Qs is shortwave radiation, Qb is net longwave radiation, Qe is latent heat flux, and Qh is sensible heat flux)) follows the seasonal pattern of the solar radiation flux. The NHF over the fresher warm pool in the SEAS is large (+70 to +130 W.m^{-2}) during mid-March to mid-April (Figure 8c). This signifies large heat gain at the sea surface contributing greatly to the SST maximum and explains the role of the low saline waters trapping the heat for the ASMWP formation. The NHF is nearly zero during mid-November to December, when the freshwaters are advected into the SEAS during winter months. The dominance of NHF among the other components of the mixed layer heat budget equation (equation (7)) is more demonstrated in Figure 9a wherein the temperature tendency (°C/month) is examined in all the components of the temperature equation. The NHF from the air-sea interaction processes (Figure 9a), contributes greatly to the increase of SST up to 2°C/month in April, the peak ASMWP period and up to 1°C–1.5°C in October, the secondary warming period of the Arabian Sea. The meridional heat advection (Figure 9a) is large in September 2005 (up to -0.5°C/month) and 2006 (up to -0.75°C/month).

[30] From Figure 9a, it is also seen that the entrainment advection is larger (up to 0.5°C/month) than the horizontal advection terms and contributes to the warming of the SST. This entrainment advection contribution appears to be overestimated. Further, it may be noted that only positive values are considered in the estimation of entrainment velocity as mentioned above. There is a somewhat inverse relation between the sea surface heat flux and the entrainment advection. In the presence of a shallow mixed layer (due to salinity stratification) embedded in a deep isothermal layer (Figure 4), one can expect entrainment advection to contribute to the observed SST variation in the SEAS.

[31] The temperature tendency (left hand side of equation (7)), the sum of the heat budget terms of equation (7) and their differences are shown in Figure 9b. Owing to overestimation of entrainment advection, the sum of the heat budget terms dominates the temperature tendency in some years and the differences are large. These differences are largely negative and could be attributed to unaccounted physical processes (including the penetrative solar radiation) as well as errors in the data sets used especially the OAFlux products. Most areas with high OAFlux discrepancies

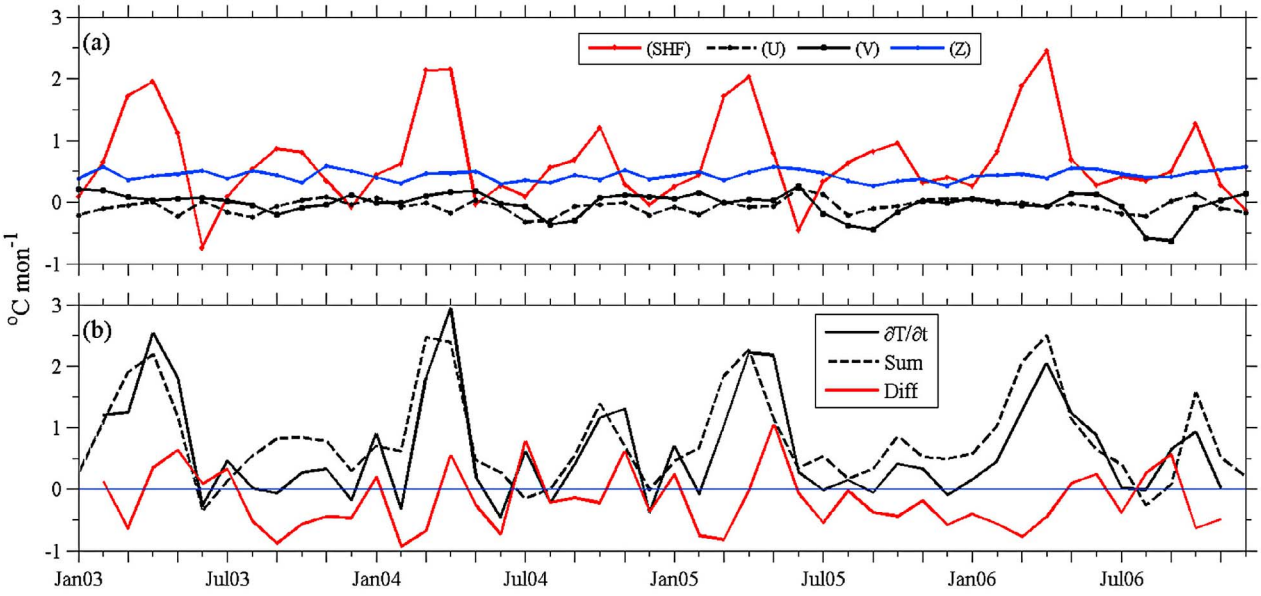

Figure 9. (a) Seasonal variation of box-averages of heat budget terms in the SEAS region (refer to white box in Figure 1). SHF is net surface heat flux, U represents zonal heat advection, V represents meridional heat advection and Z represents entrainment and (b) the heat tendency (solid black line representing the left hand side of equation (7)), the sum of heat budget terms (dashed black line representing the right hand side of equation (1)), the residual (difference between the heat tendency and the heat budget terms) equation (7).

correspond to those with the biggest SST changes [*Yu et al.*, 2007]. The large negative differences in February–March represent the occurrence of temperature inversions caused mainly by vertical salinity stratification [*Nisha et al.*, 2009]. The errors in the estimations of net heat flux that arise from the errors in the solar radiation and heat fluxes affect the first term of the right hand side of equation of equation (7). This term is also the largest contributor to the heat budget of the SEAS region.

[32] An examination of the occurrences of weather disturbances in the Arabian Sea (http://www.imd.gov.in/section/nhac/dynamic/FREQ_CYC_PREMON_SEASSON) shows that a strong monsoon onset vortex originated in the SEAS on 5 May 2004 and moved northward parallel to the west coast of India. The interannual variations of SSS and SST (Figures 3a and 3b) also showed the minimum peak SSS in February 2004 and maximum peak SST in April–May 2004 when the weather disturbance occurred. In the other years examined here, there was no monsoon vortex in

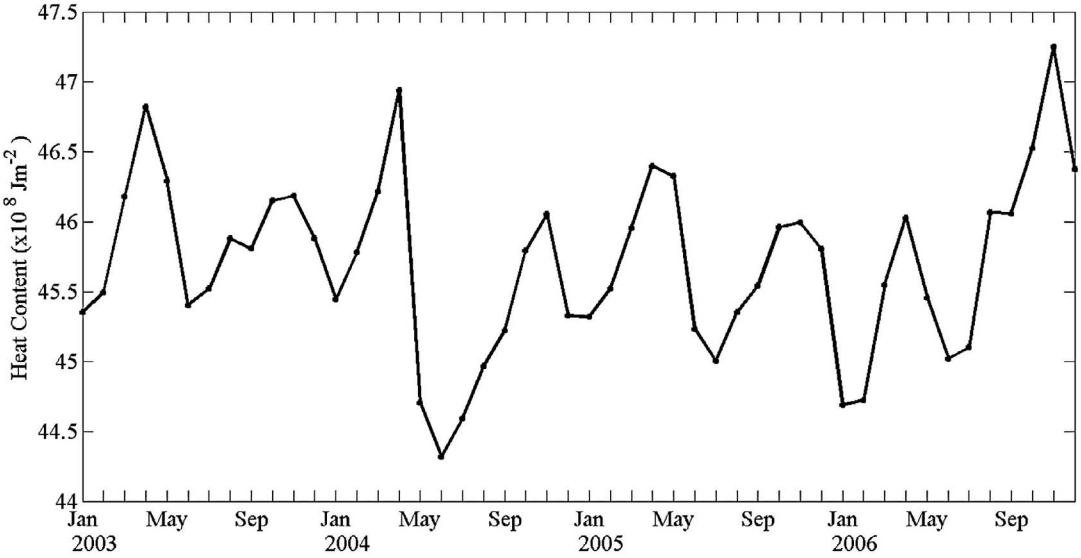

Figure 10. Seasonal variation of upper ocean heat content in the salinity-stratified layer (top 40 m) of the SEAS region computed from HYCOM simulations.

the SEAS. Though the advection of low salinity waters from the Bay of Bengal into the SEAS takes place in the winter months in each year, the reversal of the EICC in February curtails the input of low salinity waters into the SEAS (Figure 2h). However, the westward NMC from the southern Bay flows into the SEAS and advects relatively higher salinity waters, thus increasing SSS in the SEAS from February onwards (Figure 3a). The reversal of the WICC toward the equator along the coast from April (Figure 2k) also advects the northern Arabian Sea high salinity waters into the SEAS, causing SSS to continuously increase to a peak value by October–November (Figure 3a). The variability in the time of occurrence of these high salinity waters affects the salinity stratification in the following winter months and thus affects the SST variation. Though the low salinity waters are advected into the SEAS by the winter months, the mixing of these low salinity waters with the ambient high salinity waters already present in the SEAS at the end of October–November of the previous year, weakens the salinity stratification and thus SST may not increase to the peak value (e. g., SST in May 2005 and May 2006 in Figures 3a and 3b), as expected in the presence of strong salinity stratification due to trapping of heat flux in the thin mixed layer. This causes interannual variability in SST in the SEAS and modulates the upper ocean heat content variability (Figure 10) in the salinity-stratified upper 40 m layer of the ASMWP in the SEAS. It also affects the year-to-year variability in the formation of the monsoon onset vortex, an essential feature of southwest monsoon. A glance at Figure 10 shows the interesting feature of the building up of the heat content in the upper 40 m layer (47×10^8 J.m^{-2}) from January to April in 2004 that contributed to the monsoon onset vortex in May. Soon after the vortex was formed, the heat content decreased drastically to about 44.25×10^8 J.m^{-2}. Similarly, the upper ocean heat content in the upper 40 m layer was lower in the subsequent years when there was no formation of monsoon onset vortex. It is more interesting to notice larger heat content of 47.25×10^8 J m^{-2} in November 2006 which might be due to the early arrival of low salinity waters into the SEAS under the influence of the surface circulation variability and the advection of low salinity waters during the Indian Ocean Dipole Mode (IODM) event in 2006 [*Subrahmanyam et al.*, 2011].

4. Conclusions

[33] We have addressed the warm pool temperature and salinity variability in the South Eastern Arabian Sea during 2003–2006 at seasonal and interannual time scales using the high resolution HYCOM output and Argo data sets. We have also made use of the satellite derived Level 3 Sea Surface Salinity data from SMOS mission in the tropical Indian Ocean in the year 2010 and compared the SMOS SSS with that of HYCOM SSS and Argo SSS for the year 2010. The pattern of SSS variation from space agrees well with the HYCOM output SSS and Argo SSS. The HYCOM circulation and SSS together with SMOS SSS do agree with the earlier investigations on the warm pool variability in the SEAS [*Shenoi et al.*, 1999, 2005; *Vinayachandran et al.*, 2007]. We have examined the mixed layer heat budget and salt budget for 2003–2006 from HYCOM simulations and Argo data and identified the contributions of horizontal advection of low salinity waters into the SEAS during winter months (February) as a precursor to development of the intense warm pool after 2 months (April) due to dominant surface heat fluxes. The upper ocean heat content in the salinity-stratified layer contributes largely to the formation of the monsoon onset vertex and this is well evidenced in the case of monsoon onset vertex in May 2004. We have also presented the important result of this study showing that the interannual variability in the SSS in the SEAS impacts the magnitude of SST of the ASMWP. This impact on the SST in the ASMWP impacts the upper ocean heat content in the salinity-stratified layer, which then affects the variability of (formation or absence) of the monsoon onset vertex over the SEAS, prior to the southwest monsoon.

[34] This study supports the earlier investigations on the warm pool in the SEAS. Further research is needed to quantify the relationship between the upper layer heat content and the monsoon onset vortex and the processes involved in the warm pool formation in the SEAS.

[35] **Acknowledgments.** This work was supported by the Office of Naval Research (ONR) award N00014-12-1-0454 awarded to BS. BS would like to thank ESA and SMOS teams for providing the Level 2 and Level 3 Ocean Salinity data and support. The SMOS Level 3 data were obtained from the Ocean Salinity Expertise Center (CECOS) of the CNES-IFREMER Centre Aval de Traitemenent des Donnees SMOS (CATDS), at IFREMER, Plouzane (France). Special thanks to the Editor, Frank Bryan, who thoroughly reviewed the manuscript and provided useful suggestions that significantly, enhanced the quality of this paper. Finally, we wish to express our appreciation for the careful and thoughtful comments on the manuscript by three anonymous reviewers. This has the NIO contribution 5212.

References

Adler, R. F., et al. (2003), The Version-2 Global Precipitation Climatology Project (GPCP) monthly precipitation analysis (1979–present), *J. Hydrometeorol.*, *4*, 1147–1167.

Bleck, R. (2002), An oceanic general circulation model framed in hybrid isopycnic—Cartesian coordinates, *Ocean Modell.*, *37*, 55–88.

Bourassa, M. A., R. Romero, S. Smith, and J. O'Brien (2005), A new FSU winds climatology, *J. Clim.*, *18*, 3686–3698, doi:10.1175/JCLI3487.1.

Camps, A., M. Vall-Illopsserra, L. Batres, F. Torres, N. Duffo, and I. Corbella (2005), Retrieving sea surface salinity multiangular L-band brightness temperature: Improvement by spatiotemporal averaging, *Radio Sci.*, *40*, RS2003, doi:10.1029/2004RS003040.

Carnes, M. R., R. W. Helber, C. N. Barron, and J. M. Dastugue (2010), Validation test report for GDEM4, *Rep. NRL/MR/7330–10–9271*, Def. Tech. Inf. Cent., Ft. Belvoir, Va.

Chassignet, E. P., L. T. Smith, R. Bleck, and F. O. Bryan (1996), A model comparison: Numerical simulations of the north and equatorial Atlantic Oceanic circulation in depth and isopycnic coordinates, *J. Phys. Oceanogr.*, *26*(9), 1849–1867.

Delcroix, T., and C. Henin (1991), Seasonal and interannual variations of the sea surface salinity in the tropical Pacific Ocean, *J. Geophys. Res.*, *96*, 22,135–22,150, doi:10.1029/91JC02124.

Delcroix, T., and M. McPhaden (2002), Interannual sea surface salinity and temperature changes in the western Pacific warm pool during 1992–2000, *J. Geophys. Res.*, *107*(C12), 8002, doi:10.1029/2001JC000862.

Foltz, G. R., and M. J. McPhaden (2008), Seasonal mixed layer salinity balance of the tropical North Atlantic Ocean, *J. Geophys. Res.*, *113*, C02013, doi:10.1029/2007JC004178.

Font, J., G. Lagerloef, and D. Le Vine (2004), The determination of surface salinity with the European SMOS space mission, *IEEE Trans. Geosci. Remote Sens.*, *42*, 2196–2205.

Font, J., A. Camps, M. Borges, M. Martin-Neira, J. Boutin, N. Reul, Y. H. Kerr, A. Hahne, and S. Mecklenberg (2010), SMOS: The challenging sea surface salinity measurements from space, *Proc. IEEE*, *98*, 649–665.

Gadgil, S., P. V. Joseph, and N. V. Joshi (1984), Ocean atmosphere coupling over monsoon regions, *Nature*, *312*, 141–143.

Hareeshkumar, P. V., P. Madhusoodanan, M. P. Ajai Kumar, and A. Raghunadha Rao (2005), Characteristics of Arabian Sea mini warm pool during May 2003, *Mausam*, *56*, 169–174.

Huang, B., and V. M. Mehta (2004), Response of the Indo-Pacific warm pool to interannual variations in net atmospheric freshwater, *J. Geophys. Res.*, *109*, C06022, doi:10.1029/2003JC002114.

Huang, B., Y. Xue, and D. W. Behringer (2008), Impacts of Argo salinity in NCEP Global Ocean Data Assimilation System: The tropical Indian Ocean, *J. Geophys. Res.*, *113*, C08002, doi:10.1029/2007JC004388.

Joseph, S., and H. J. Freeland (2005), Salinity variability in the Arabian Sea, *Geophys. Res. Lett.*, *32*, L09607, doi:10.1029/2005GL022972.

Kobayashi, T., and S. Minato (2005), What observation scheme should we use for profiling floats to achieve the Argo goal for salinity measurement accuracy? Suggestions from software calibration, *J. Atmos. Oceanic Technol.*, *22*, 1588–1601.

Krishna Kumar, K., M. Hoerling, and B. Rajagopalan (2005), Advancing dynamical prediction of Indian monsoon rainfall, *Geophys. Res. Lett.*, *32*, L08704, doi:10.1029/2004GL021979.

Kurian, J., and P. N. Vinayachandran (2007), Mechanisms of formation of the Arabian Sea mini warm pool in a high-resolution Ocean General Circulation Model, *J. Geophys. Res.*, *112*, C05009, doi:10.1029/2006JC003631.

Large, W. G., J. C. McWilliams, and S. C. Doney (1994), Oceanic vertical mixing: A review and a model with a nonlocal boundary layer parameterization, *Rev. Geophys.*, *32*(4), 363–403.

McPhaden, M. J., G. R. Foltz, T. Lee, V. S. N. Murty, M. Ravichandran, V. Gabriel, J. Vialard, J. D. Wiggert, and Y. Lisan (2009), Ocean-atmosphere interactions during cyclone Nargis, *Eos Trans. AGU*, *90*(7), 53–54.

Morrison, J. (1997), Inter-monsoonal changes in the T-S properties of the near-surface waters of the northern Arabian Sea, *Geophys. Res. Lett.*, *24*, 2553–2556.

Murty, V. S. N., S. M. Krishna, A. Nagaraju, Y. K. Somayajulu, V. Ramesh Babu, D. Sengupta, P. R. Sindu, M. Ravichandran, and G. Rajesh (2006), On the warm pool dynamics in the southeastern Arabian Sea during April–May 2005 based on the satellite remote sensing and ARGO float data, *Proc. SPIE*, *4606*, 1–12, doi:10.1117/12.694254.

Nisha, K., et al. (2009), Reduced near-surface thermal inversions in 2005–06 in the southeastern Arabian Sea (Lakshadweep Sea), *J. Phys. Oceanogr.*, *39*, 1184–1199.

Nyadjro, E. S., B. Subrahmanyam, V. S. N. Murty, and J. F. Shriver (2010), Salt transport in the near-surface layer in the monsoon-influenced Indian Ocean using HYCOM, *Geophys. Res. Lett.*, *37*, L15603, doi:10.1029/2010GL044127.

Nyadjro, E. S., B. Subrahmanyam, and J. F. Shriver (2011), Seasonal variability of salt transport during the Indian Ocean monsoons, *J. Geophys. Res.*, *116*, C08036, doi:10.1029/2011JC006993.

Oliva, R., E. Daganzo-Eusebio, Y. H. Kerr, S. Mecklenburg, S. Nieto, P. Richaume, and C. Gruhier (2012), SMOS radio frequency interference scenario: Status and actions taken to improve the RFI environment in the 1400–1427-MHz passive band, *IEEE Trans. Geosci. Remote Sens.*, *50*, 1427–1439.

Prasad, T. G., and M. Ikeda (2002), A numerical study of the seasonal variability of Arabian Sea high-salinity water, *J. Geophys. Res.*, *107*(C11), 3197, doi:10.1029/2001JC001139.

Rao, R. R., and R. Sivakumar (1999), On the possible mechanism of the evolution of a mini-warm pool during the pre-monsoon season and the onset vortex in the Southeastern Arabian Sea, *Q. J. R. Meteorol. Soc.*, *125*, 787–809.

Rao, R. R., and R. Sivakumar (2003), Seasonal variability of sea surface salinity and salt budget of the mixed layer of the north Indian Ocean, *J. Geophys. Res.*, *108*(C1), 3009, doi:10.1029/2001JC000907.

Ren, L., and S. C. Riser (2009), Seasonal salt budget in the northeast Pacific Ocean, *J. Geophys. Res.*, *114*, C12004, doi:10.1029/2009JC005307.

Riser, S., L. Ren, and A. Wong (2008), Salinity in Argo: A modern view of a changing ocean, *Oceanography*, *21*, 56–67.

Schott, F. A., and J. P. McCreary Jr. (2001), The monsoon circulation of the Indian Ocean, *Prog. Oceanogr.*, *51*, 1–123.

Sengupta, D., S. R. Parampil, G. S. Bhat, V. S. N. Murty, V. Ramesh Babu, T. Sudhakar, K. Premkumar, and Y. Pradhan (2008), Warm pool thermodynamics from the Arabian Sea Monsoon Experiment (ARMEX), *J. Geophys. Res.*, *113*, C10008, doi:10.1029/2007JC004623.

Shenoi, S. S. C., D. Shankar, and S. R. Shetye (1999), The sea surface temperature high in the Lakshadweep Sea before the onset of the southwest monsoon, *J. Geophys. Res.*, *104*, 703–712.

Shenoi, S. S. C., D. Shankar, V. V. Gopalakrishna, and F. Durand (2005), Role of ocean in the genesis and annihilation of the core of the warm pool in the southeastern Arabian Sea, *Mausam*, *56*(1), 147–161.

Stevenson, J. W., and P. P. Niiler (1983), Upper ocean heat budget during the Hawaii-to-Tahiti shuttle experiment, *J. Phys. Oceanogr.*, *13*, 1894–1907.

Subrahmanyam, B., V. S. N. Murty, and D. M. Heffner (2011), Sea surface salinity variability in the tropical Indian Ocean, *Remote Sens. Environ.*, *115*(3), 944–956.

Subrahmanyam, B., G. Grunseich, and E. S. Nyadjro (2012), Preliminary SMOS salinity measurements and validation in the Indian Ocean, *IEEE Trans. Geosci. Remote Sens.*, *PP*(99), 1–9.

Swenson, M. S., and D. V. Hansen (1999), Tropical Pacific Ocean mixed layer heat budget: The Pacific cold tongue, *J. Phys. Oceanogr.*, *29*, 69–81.

Vinayachandran, P. N., and S. R. Shetye (1991), The warm pool in the Indian Ocean, *Proc. Indiana Acad. Sci.*, *100*, 165–175.

Vinayachandran, P. N., Y. Masumoto, T. Mikawa, and T. Yamagata (1999), Intrusion of the southwest monsoon current into the Bay of Bengal, *J. Geophys. Res.*, *104*, 11,077–11,085.

Vinayachandran, P. N., J. Kurian, and C. P. Neema (2007), Indian Ocean response to anomalous conditions in 2006, *Geophys. Res. Lett.*, *34*, L15602, doi:10.1029/2007GL030194.

Waliser, D. E. (1996), Formation and limiting mechanisms for very high sea surface temperature: Linking the dynamics and the thermodynamics, *J. Clim.*, *9*, 161–188.

Wong, A. P. S., G. C. Johnson, and W. B. Owens (2003), Delayed-mode calibration of autonomous CTD profiling float salinity data by θ–S climatology, *J. Atmos. Oceanic Technol.*, *20*, 308–318.

Yu, L., X. Jin, and R. A. Weller (2007), Annual, seasonal, and interannual variability of air-sea heat fluxes in the Indian Ocean, *J. Clim.*, *20*, 3190–3209.